# Parameter Estimation Accuracy in Hybrid Gravitational Waveform Modeling

Zach Hafen

August 2013

**Abstract**

There exist a number of models describing the gravitational wave signals produced by coalescing compact binaries, including a group of phenomenological models calibrated with "hybrid" waveforms. We examine how accurate these models need to be in order to avoid adversly affecting parameter estimation for equal-mass non-spinning binary black hole systems. We do this by "injecting" a hybrid waveform as a source and attempting to recover it with a variety of template waveforms. The template waveforms use the same waveform as the source, but may have different parameters and may be altered in a way that mocks up the error we expect hybrid waveforms to have. We then track and interpret changes in the parameters of the template waveforms that are most successful at recovering the source waveform.

## Contents



## 1 Introduction

Gravitational waves are ripples in the fabric of space and time caused by the acceleration of masses. Since they are extremely small in magnitude they can only be detected when a very sensitive detector is used to observe massive sources. (For a good introduction to gravitational waves, see [12].) There

is a major international effort to detect gravitational waves which is finally bearing fruit — when the advanced LIGO and VIRGO detectors become operational within the next few years we hope to detect gravitational waves from a variety of extrasolar sources. Successful detections would provide the most stringent test to date of Einstein's theory of general relativity, yield information about the distribution of black holes and other massive objects in our universe, reveal more about extrasolar events like supernovae, and maybe produce other discoveries which cannot be predicted.

Among the sources we hope to detect are coalescing compact binaries. These consist of either a neutron star and a neutron star, a neutron star and a black hole, or a black hole and a black hole orbiting each other and eventually colliding. The gravitational waves produced by coalescing compact binaries are particularly appetizing to study because they create sufficiently large gravitiational waves, depend on relatively few parameters, are predictable enough to use matched filtering on, and can contain many cycles in the frequency range advanced LIGO and VIRGO are tuned for [3]. Due to these traits, a significant effort has gone into building models describing the signals produced by coalescing compact binaries and assessing the accuracy of said models. There already exist sufficient error criterion to determine if a model is accurate enough to be used to detect an event as pointed out by [7] and others. Less work has been done to assess how accurate a model needs to be to extract useful information about the parameters of the sourcesm, which is the primary goal of this work. In particular, we will focus on parameter estimation accuracy requirements for binary black hole (BBH) systems, much of which can be extended to neutron star-black hole binaries and neutron star-neutron star binaries. We will further narrow down our focus to a particular type of waveform modeling.

In the remainder of the the introduction we go over a brief overview of matched filtering and waveform modeling for BBH systems. In the methods section we discuss the process of "injecting" waveforms and grid-based searches before moving on to the specific modified waveforms we use and the results of using them. The discussion section goes over some of the implications of these results along with future plans and limitations to the method used. We finish with acknowledgments and references.

## 1.1 Gravitational waveform modeling for BBH systems

The gravitational waves produced by BBH systems as seen by the detectors depend on $\sim$15 parameters — including the masses and spins of the black holes, the distance to the black holes, the orientation of the orbital plane, the location in the sky, and the initial time and phase of observation. The signals have three phases in their lifetime: inspiral, merger, and ringdown. During the inspiral phase the two blackholes orbit around each other in a stable orbit with steadily decreasing radius. The black holes then merge in the next phase, and finally in the ringdown phase any perturbations in the new black hole are bled out.

In order to model this behavior, post-Newtonian (PN) approximations and numerical relativity (NR) simulations are used (as well as perturbation theory for the ringdown phase). PN approximants are slow motion, asymptotic expansions in terms of the relative velocity of the black holes $v/c$. They lose accuracy as the black holes get closer to merger and $v$ increases. NR simulations are discrete solutions to the Einstein field equations. While NR simulations are sufficiently accurate they are also computationally expensive, especially for larger seperation distances, spins, and mass ratios. As such, they generally start at the end of the gravitational wave signal and continue down to some time in the inspiral shortly before merger.

One way of making use of these two methods is to combine them into a "hybrid" waveform.

Hybrid waveforms take a PN approximant for the earlier part of the gravitational wave signal, a NR simulation for the later part, and stitch them together around some matching frequency $\omega_m$ in the middle by utilizing a free time and phase shift. This limits the use of PN or NR methods in the regimes where they are less viable. Hybrid waveforms are then used to calibrate phenomenological models, such as IMRPhenomB [1] and IMRPhenomC [11]. Another technique that uses PN and NR methods are effective-one-body numerical relativity (EOBNR) models (for example [4, 10]). EOBNR models use NR data to extend and inform analytical expressions. Ohme [9] provides a brief and informative overview of the current state of BBH modeling.

Phenomenological models calibrated using hybrid waveforms are the focus of our work — in particular we use IMRPhenomB. Past studies (including but not limited to [2, 3, 5, 6, 7, 9]) have revealed information about the overal accuracy of hybrid waveforms as well as the individual pieces of hybrid waveforms. From these we know that there some error in the hybrid waveforms is due to error in the NR simulation and error in the process of stitching the NR and PN parts together, but that the majority of the error in hybrid waveforms comes from the PN portion of the waveform [7]. One way to limit this inaccuracy is to increase the length of the NR portion of the waveform. Since this is computationally expensive, an effort has been made to determine the minimum necessary length of NR data runs needed to insure sufficient accuracy [5, 7]. There are also multiple types of PN approximants, and the accuracy of the approximant has been shown to be dependent on the mass ratio used [6].

## 1.2 Matched filtering

Although the advanced LIGO and VIRGO detectors are very sensitive, the noise in the detectors is expected to dominate over the gravitational wave signals. In order to extract a gravitational wave signal from this noise, we use matched filtering. Matched filtering allows us to check if there is a signal with a given form contained in the data, provided we know what that form is beforehand. In order to do this we look at the noise-weighted inner product of two time-domain waveforms $h_1$ and $h_2$, defined as

$$\langle h_1|h_2\rangle = 4Re\int_{f_{min}}^{f_{max}} \frac{\tilde{h}_1(f)\tilde{h}_2^*(f)}{S_n(f)}df. \tag{1}$$

Here the tilda denotes the fourier transform of the respective time-domain waveform, $f_{min}$ and $f_{max}$ describe the interval the detector is sensitive over, and $S_n(f)$ is the power spectral density of the detector noise. For our work we calculate $S_n(f)$ from the zero-detuned, high-power advanced LIGO noise curve (ZERO_DET_high_P in [13]).

Consider some data $d(t)$ composed of a gravitational wave signal $s(t)$ and some noise $n(t)$ such that $d(t) = s(t)+n(t)$.We might then investigate how much of a template waveform $h(t,\vec{\theta})$ is in $d(t)$ (Here $\vec{\theta}$ is a vector in the template's parameter space that describes the specific set of parameters used to calculate the template waveform.) This can be done by calculating the signal-to-noise ratio (SNR($\vec{\theta}$)), which is

$$\text{SNR}(\vec{\theta}) = \frac{\langle h(\vec{\theta})|d\rangle}{\sqrt{\langle h(\vec{\theta})|h(\vec{\theta})\rangle}}. \tag{2}$$

Maximized SNR's for a given template as high as ∼60 will possibly be detected, but a more standard SNR will be on the order of ∼10. (For a pleasant derivation of (1) and (2) see [8].) Another useful

measure of examining differences in waveforms is the overlap $\mathcal{O}(\vec{\theta})$,

$$\mathcal{O}(\vec{\theta}) = max_{t_0,\phi_0} \frac{\langle h(\vec{\theta})|d\rangle}{\sqrt{\langle h(\vec{\theta})|h(\vec{\theta})\rangle\langle d|d\rangle}} = 1 - \mathcal{M}(\vec{\theta}). \tag{3}$$

In terms of the SNR, the overlap is a normalized SNR maximized over the initial time and phase ($t_0$ and $\phi_0$ respectively) of the template waveform. It is related in (3) to the frequently used mismatch $\mathcal{M}(\vec{\theta})$.

For parameter estimation, a more statistical approach is also useful. Such approaches often make use of the likelihood $L(\vec{\theta})$. Here the likelihood that for a specific $\vec{\theta}$ we have a waveform described by $d(t)$ is

$$L(\vec{\theta}) = P(d|\vec{\theta}) = \exp\left(\frac{\langle d - h(\vec{\theta})|d - h(\vec{\theta})\rangle}{2}\right). \tag{4}$$

Assuming a uniform prior $P(\vec{\theta})$, the probability $P(\vec{\theta}|d)$ that given $d(t)$ is described by $\vec{\theta}$ is then

$$P(\vec{\theta}|d) \propto P(d|\vec{\theta})P(\vec{\theta}) = \mathcal{N}\exp\left(\langle h(\vec{\theta})|d\rangle - \frac{\langle h(\vec{\theta})|h(\vec{\theta})\rangle}{2}\right), \tag{5}$$

where $\mathcal{N}$ is some normalization constant. The parameters can then be estimated by finding the value of $\vec{\theta}$ that maximizes (5). A useful discussion on parameter estimation is again provided by [8].

## 2 Method

Since gravitational waves have yet to be detected, a common practice in assessing the accuracy of waveforms is to set $s(t)$ as a waveform thought to be reasonably correct. (This is generally referred to as "injecting" a signal.) If the injected waveform is trusted to be sufficiently accurate, the errors that result from incorrectly modeling the injected waveform are expected to be similar to errors that result from incorrectly modeling a true gravitational waveform. For our work we use stationary, gaussian noise that averages to zero ($n(t) = 0$ and therefore $d(t) = s(t)$).

To compare a template waveform with an injected waveform for different values of $\vec{\theta}$ we perform a grid-based search, or "gridsearch", over a section of parameter space. In a gridsearch we calculate the SNR, the overlap, and/or the likelihood for various $\vec{\theta}$'s located on a grid in the parameter space.

For our gridsearches we inject an IMRPhenomB waveform by Ajith et al. [1] and use either a modified or unmodified IMRPhenomB waveform as the template. IMRPhenomB depends on the total mass of the system $M_{total}$, the symmetric mass ratio $\left(\eta \equiv \frac{M_1 M_2}{(M_1+M_2)^2}\right)$, a spin parameter that accounts for the spin of both black holes, the initial time and phase of observation, and the effective distance to the source (which includes the sky location, the orientation of the orbital plane, and the distance to the source). We limit our study to injected waveforms for equal-mass non-spinning binaries with a total mass of between 10 and 40 $M_\odot$ at an effective distance of 100 Mpc and with no initial time or phase offset.

For our template waveforms we maximize the overlap, SNR, or likelihood (depending on the type of gridsearch) over time and phase, we set the effective distance to the effective distance of the injected waveform, and we use only non-spinning templates. This leaves $M_{total}$ and $\eta$ as unassigned parameters to perform the gridsearch over. (There may also be parameters in the template waveform

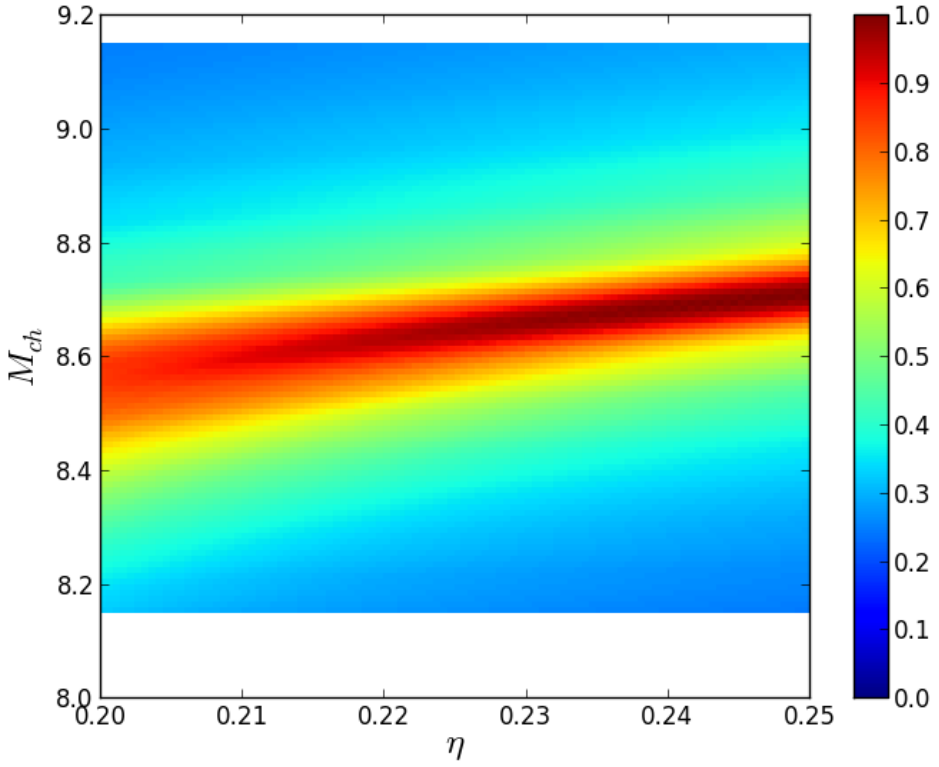


Figure 1: An overlap gridsearch performed with the template waveform varied over $\eta$ and $M_{ch}$. The source is a 10-10 $M_{\odot}$ BBH.

introduced by modifying IMRPhenomB, but since such parameters describe errors in the process of modeling and not different sources we did not perform gridsearches over them.) A gridsearch over $M_{total}$ and $\eta$ can be done over $\eta$ and the chirp mass $\left(M_{ch} \equiv \frac{(M_1 M_2)^{3/5}}{(M_1+M_2)^{1/5}}\right)$ instead, since there is a one-to-one conversion between the two. (This is desirable because $M_{ch}$ features prominently in form of the PN approximants.)

We show a standard overlap gridsearch that uses an unmodified IMRPhenomB template waveform in Figure 1. For brevity, we refer to gridsearches that use unmodified IMRPhenomB template waveforms as "unmodified" gridsearches and vice-versa for ones that use a modified IMRPhenomB template waveform. Figure 2 shows six unmodified overlap gridsearches performed for different total masses. The gridsearches in Figure 2 focus on higher overlap values, so anything below an overlap of .90 shows only as dark blue. All gridsearches use 20 Hz as $f_{min}$ and the highest frequency over the entire grid at which the template waveform goes to zero as $f_{max}$. We use the unmodified gridsearches as bases to compare modified gridsearches against.

As a quick note, we cannot entirely trust the values of our gridsearches due to statistical uncertainty, but in practice are limited to considering regions we are confident to some percentage contain the parameters that describe the true waveform. Baird et al. [2] suggest that as a rough approximation for high SNRs, we can be 90% sure that the parameters that describe a source waveform are contained within the .97 overlap contour for a gridsearch.

## 2.1 Three-stage Modified IMRPhenomB

To estimate the effects of an incorrect waveform on parameter estimation we modify IMRPhenomB to simulate errors. When a waveform differs from nature's waveform its phase evolution progresses differently, therefore creating an erroneous phase- or time-shift. We parametrize our modified waveforms over the erroneous phase- or time-shift ($\alpha$ and $\tau$ respectively) that occurs between two frequencies $f_{low}$ and $f_{high}$. For our first modified waveform, referred to as the three-stage modified IMRPhenomB, we add no modifications before $f_{low}$, increase $\alpha$ or $\tau$ uniformly between $f_{low}$ and $f_{high}$, and keep $\alpha$ or $\tau$ at a constant value past $f_{high}$. The fourier transform of the three-stage modified IMRPhenomB waveform[1] is

$$\tilde{h}_T(f) \equiv \begin{cases} \tilde{h}_{unmod}(f), & f < f_{low} \\ e^{-iQ(f)(\alpha+f\tau)}\tilde{h}_{unmod}(f), & f_{low} \leq f \leq f_{high} \\ e^{-i(\alpha+f\tau)}\tilde{h}_{unmod}(f), & f_{high} < f. \end{cases} \tag{6}$$

Where $\tilde{h}_{unmod}(f)$ is the fourier transform of the unmodified IMRPhenomB waveform, and $Q(f)$ is a linear scaling function, $Q(f) \equiv \frac{f-f_{low}}{f_{high}-f_{low}}$.

For various values of $\alpha$ and $\tau$ we perform modified overlap gridsearches using $\tilde{h}_T(f)$ as our template waveform. These gridsearches address the error accumulated by an incorrect waveform between the lowest frequency the detector is sensitive to a frequency NR simulations are expected to reach. This corresponds to a $f_{low}$ equal to $f_{min}$ and a $f_{high}$ calculated from $M_{total}\Omega_{high} = .042$ ($f_{high} = \frac{.042}{2\pi M_{total}}$). We vary $\alpha$ between -1.0 and 1.0 rad while holding $\tau$ at zero, and $\tau$ between -.05 and .05 seconds while holding $\alpha$ at zero.

To compare the modified gridsearches to the unmodified ones we look at the location of the modified gridsearch's best fit. If a template waveform exactly matches the injected waveform, the

[1] This waveform was originally suggested by Harald Pfeiffer.

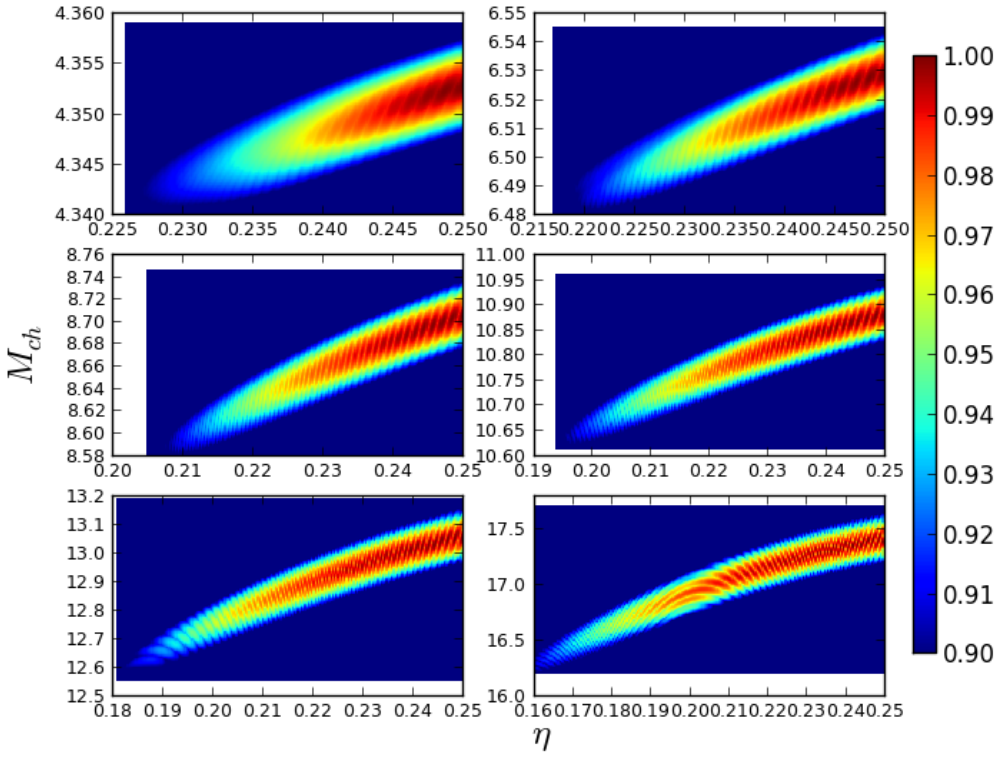


Figure 2: Unmodified overlap gridsearches for various total masses. The top row contains gridsearches for a total mass of 10 and 15 $M_\odot$ on the left and right respectively. The middle row contains gridsearches for a total mass of 20 and 25 $M_\odot$. The bottom row contains gridsearches for a total mass of 30 and 40 $M_\odot$.

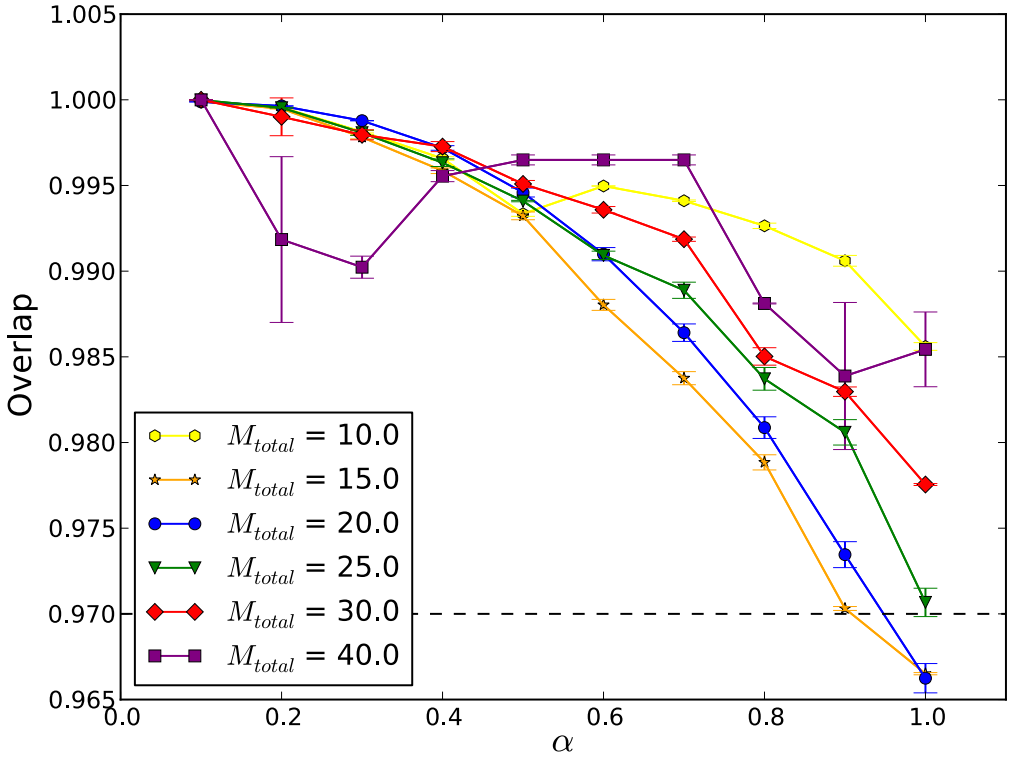


Figure 3: Overlap contour plot for increasing $\alpha$. The dashed line indicates the .97 overlap contour. The total mass in solar masses for each series of modified gridsearches is given in the key.

parameters used to create the template waveform at the best fit will also be the parameters used to create the injected wavorm (provided $n(t) = 0$). If the template waveform does not completely match the injected waveform then this will not be the case, and the best-fit will be at a different location in the parameter-space. The difference in location is an estimate of systematic bias built into the gridsearch. Using the approximation mentioned above, if the location of the best fit for a modified gridsearch is still within an unmodified gridsearch's .97 overlap contour, the statistical uncertainty exceeds the systematic bias. When the best fit falls outside the .97 overlap contour the systematic biases contributed by the template waveform are certainly worth considering.

As we increase the magnitude of $\alpha$ or $\tau$ we track the location of the modified gridsearch's best fit in the $\eta$-$M_{ch}$ plane, as well as the overlap of the unmodified gridsearch at that point. Similar to the unmodified gridsearches in Figure 2, there are many local extrema in a given modified gridsearch. These extrema are often very similar in height while the values around them quickly drop off, allowing an incorrect estimation of the area the best fit is near. This can be a large distance in the $\eta$-$M_{ch}$ plane, and can therefore significantly affect results. To correct for this, we

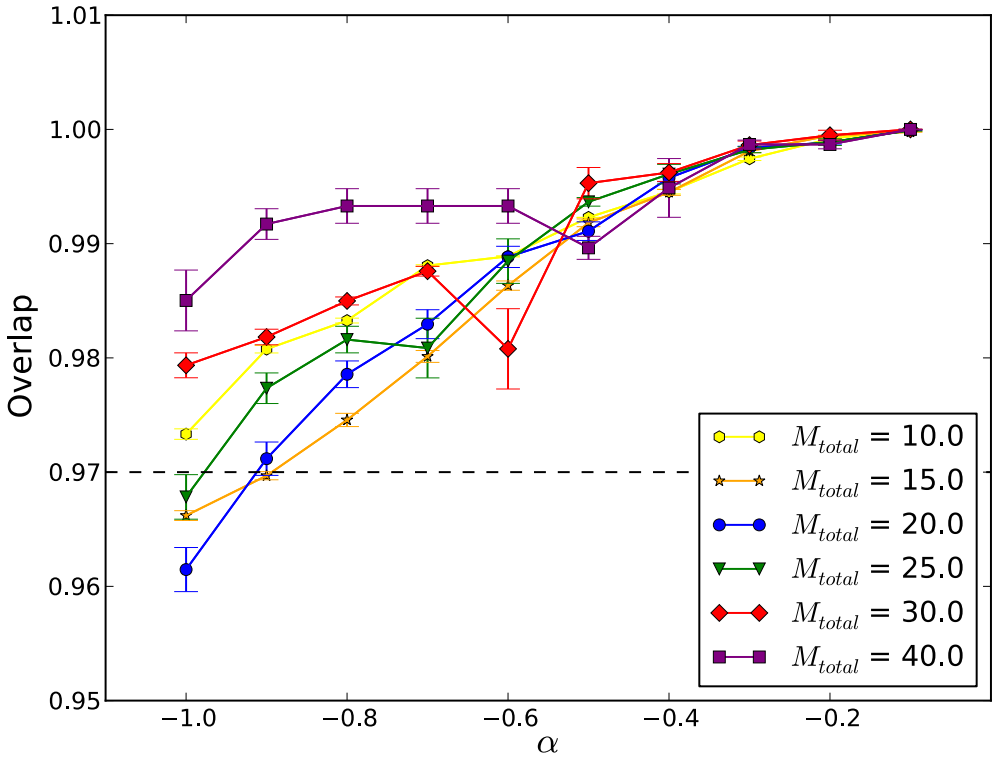


Figure 4: Overlap contour plot for decreasing $\alpha$

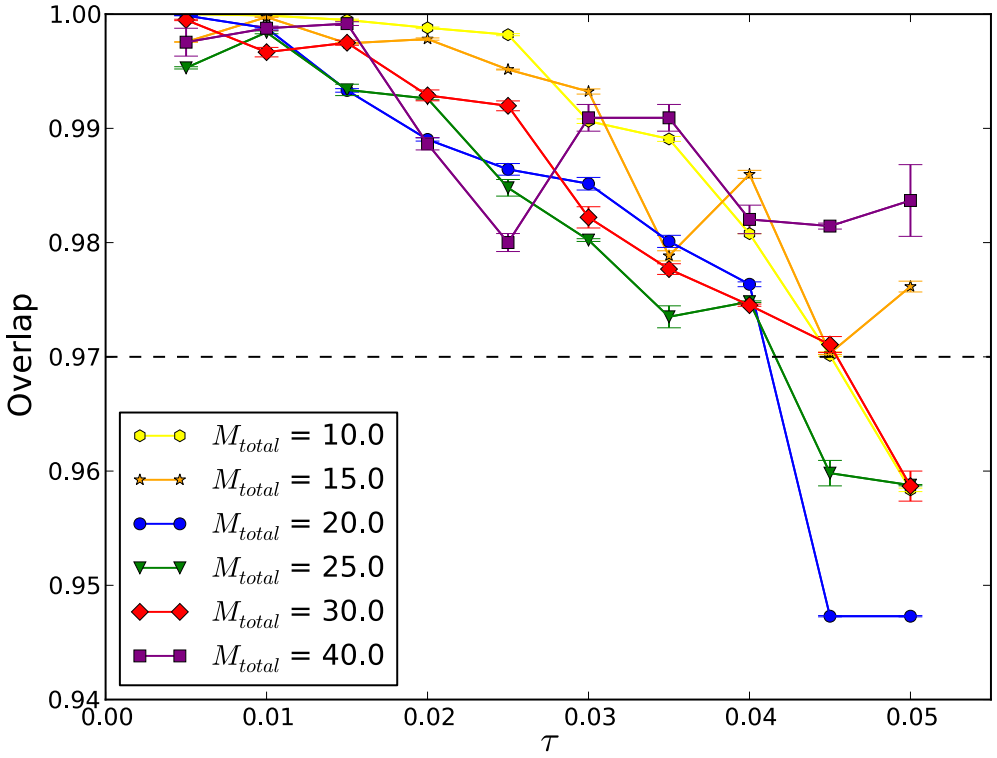


Figure 5: Overlap contour plot for increasing $\tau$.

created smaller and denser gridsearches around the best fit and the second highest value on the gridsearch. From these we selected the new highest value as the "true" best fit. Figures 3 and 4 plot the the unmodified gridsearch overlap value at the location of the best fit versus the $\alpha$ value used in generating the modified gridsearch. Figures 5 and 6 show the same for various $\tau$'s. The paths traced out by the best fit as $\alpha$ is varied positively for a $M_{total}$ of 20 and 25 $M_{\odot}$ are shown in Figure 11. All the best fit paths are found in in the Appendix.

## 2.2 PN-term Modified IMRPhenomB

Our second modified waveform, the PN-term modified IMRPhenomB, focuses on the effects of error accumulated in the PN phase description. The unmodified phase [1] of IMRPhenomB is

$$\Psi(f) \equiv 2\pi f t_0 + \phi_0 + \frac{3}{128\eta\nu^5}\left(1 + \sum_{k=2}^{7} \nu^k \psi_k\right). \tag{7}$$

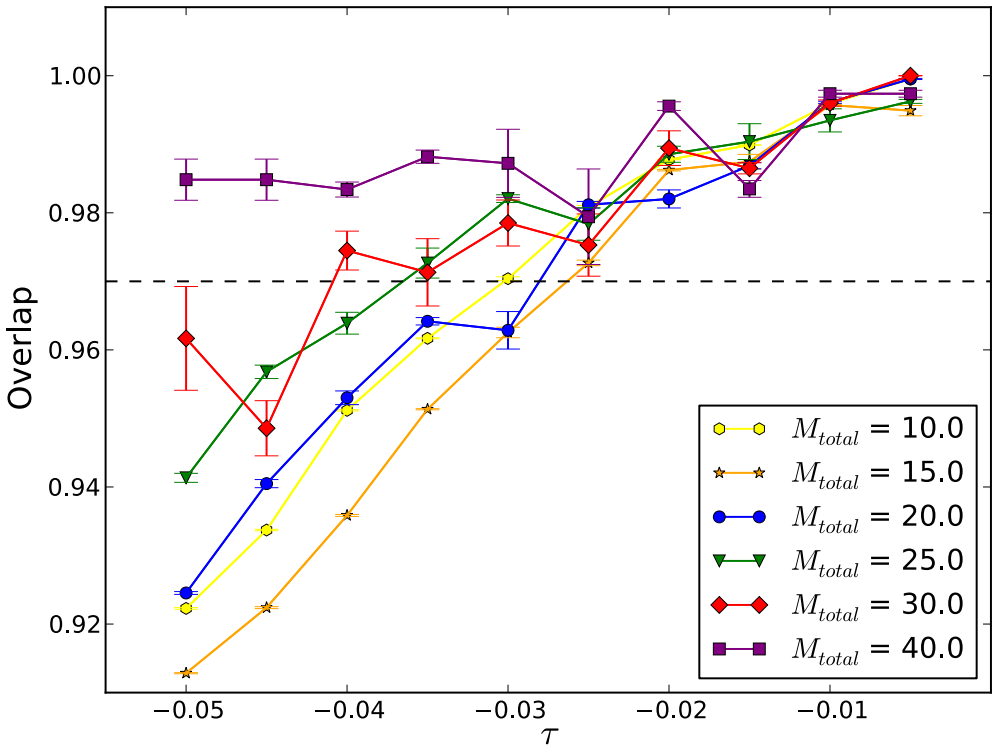


Figure 6: Overlap contour plot for decreasing $\tau$

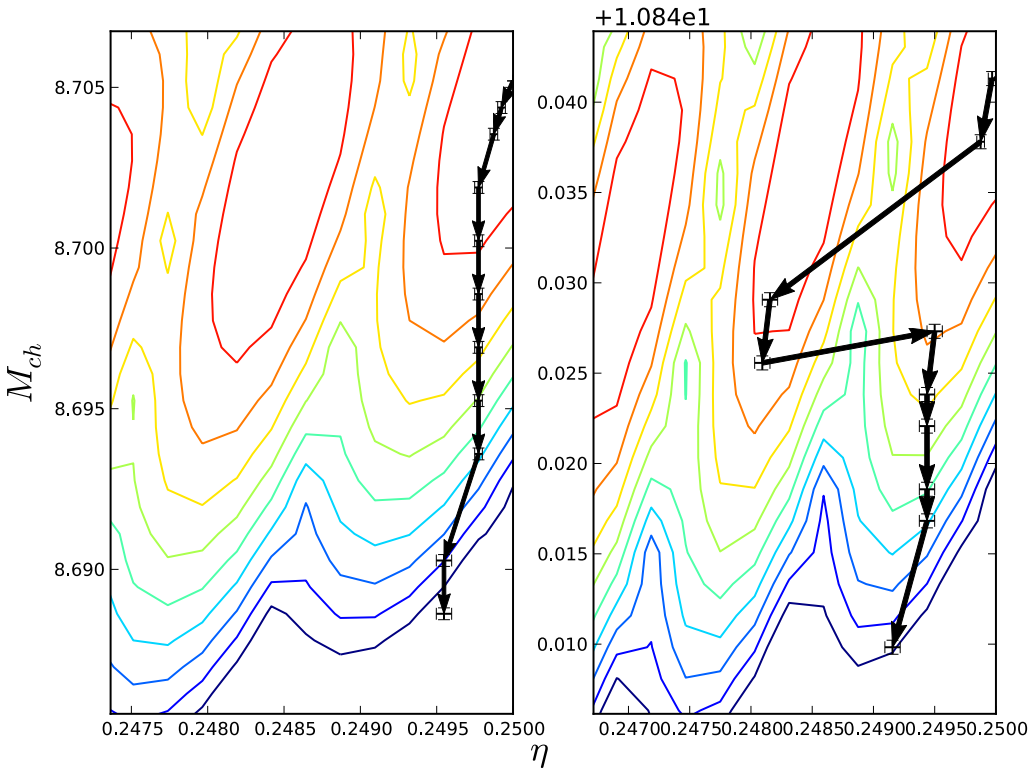


Figure 7: Best fit path plots for $M_{total}$ of 20 and 25 $M_{\odot}$ (left and right respectivly). We vary $\alpha$ from 0.0 to 1.0 rad in increments of 0.1 rad.

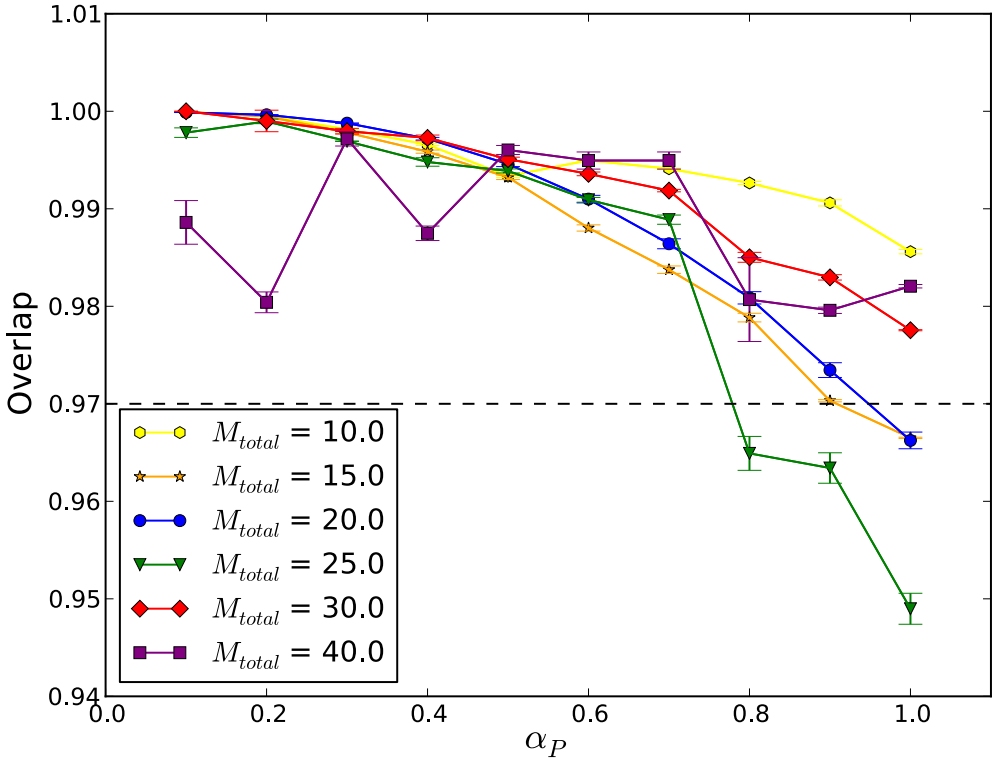


Figure 8: Overlap contour plot for increasing $\alpha_P$.

Where $\nu = (\pi M_{total} f)^{1/3}$, $\psi_k$ are various constants, and $\nu^k \psi_k$ corresponds to the $k/2$ PN order correction term (for instance, $\nu^7 \psi_7$ corresponds to the 3.5 order PN term). We introduce error as a 4.0 order PN term, $\nu^8 \psi_8$, with the constant $\psi_8$ parametrized by $\alpha_P$, the erroneous phase difference accumulated betwen $f_{low}$ and $f_{high}$. The PN-term modified IMRPhenomB is

$$\tilde{h}_{PNmod}(f) \equiv \begin{cases} \exp\left(\frac{-i3\nu(f)^3\psi_8}{128\eta}\right)\tilde{h}_{unmod}(f), & f \leq f_{high} \\ \exp\left(\frac{-i3\nu_{high}^3\psi_8}{128\eta}\right)\tilde{h}_{unmod}(f), & f_{high} < f, \end{cases} \tag{8}$$

$$\psi_8 \equiv \frac{128\eta\alpha_P}{3(\nu_{high}^3 - \nu_{low}^3)}. \tag{9}$$

We define $\nu_{high} \equiv \nu(f_{high})$ and $\nu_{low} \equiv \nu(f_{low})$. We repeat the same modified procedure we use for the three-stage modified IMRPhenomB by varying $\alpha_P$ between -1.0 and 1.0 rad, with the results displayed in Figures 8 and 9.

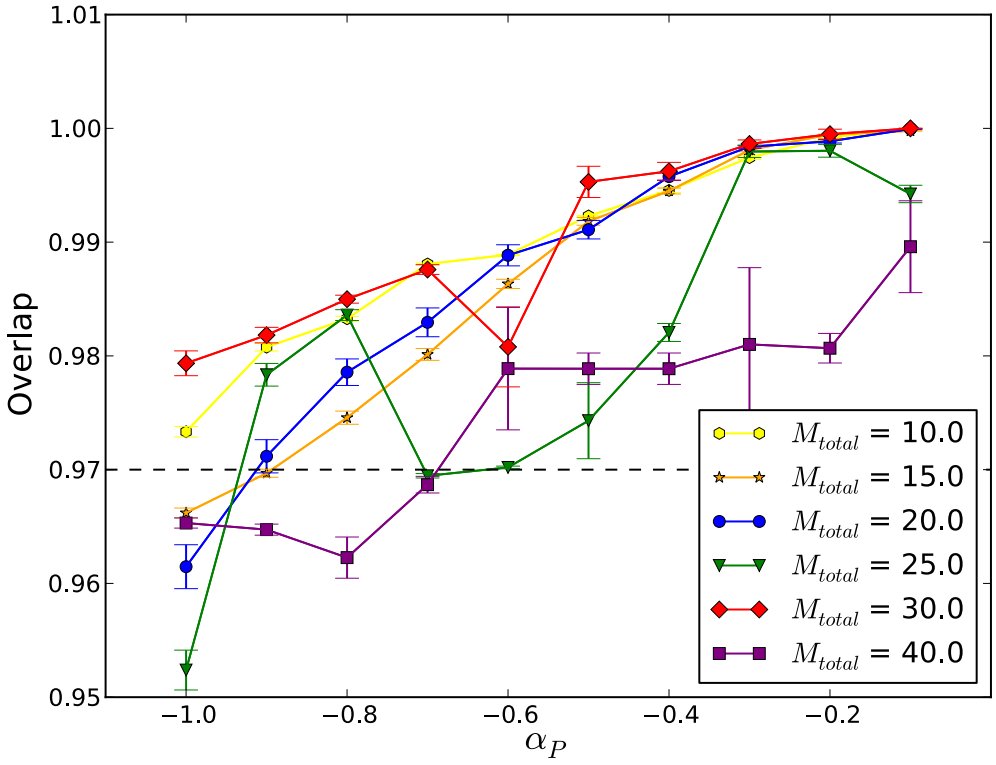


Figure 9: Overlap contour plot for decreasing $\alpha_P$

# 3 Discussion

By creating modified versions of a waveform and comparing them to unmodified waveforms we have attempted to simulate the type of disagreements we might expect between a model waveform and a waveform produced by nature. In our study we limited our efforts to equal-mass, non-spinning BBH systems. We focused on error accumulated between the start of the detector's sensitivity range at 20 Hz and our estimate for a frequency future NR runs might go down to, $M_{total}\Omega_{high} = .042$. The three-stage modified IMRPhenomB added the error in the modified waveform uniformly over our region of interest, while our PN-term modified IMRPhenomB added the error as a user-specified 4.0 PN term.

Figures 3 and 4 reveal that three-stage modified gridsearches varied over $\alpha$ the gridsearches with a $M_{total}$ value of 15 or 20 $M_{\odot}$ exit the .97 overlap contour first with a magnitude of $\sim$0.9 rad for both positive and negative $\alpha$'s, while gridsearches with other total masses exit later. Figures 5 and 6 show the best fits exiting the .97 overlap contour at a similar yet erratic rate. For three-stage modified gridsearches varied over $\tau$, the earliest exit for positive $\tau$ is $\sim$0.04 seconds and the earliest exit for negative $\tau$ has a magnitude of $\sim$0.025 seconds. These correspond to an accumulated phase difference between $f_{low}$ and $f_{high}$ of $\sim$2.7 and $\sim$2.3 rad respectively.

From Figures 8 and 9 we observe for a PN-term modified gridsearch varied over $\alpha_P$, the earliest positive exit is for a $M_{total}$ of 25 $M_{\odot}$ and an $\alpha_P$ of $\sim$0.7 and the earliest negative exit is for the same total mass and an $\alpha_P$ of magnitude $\sim$0.6. If we take the lowest phase difference that causes the best fit to exit the .97 contour across both modified waveforms as a rough estimate for a lower limit, we can see that for modeled waveforms with an erroneous phase difference less than $\sim$0.6 the statistical uncertainty is greater than the systematic bias produced. Similarly, modeled waveforms with an erroneous time difference less than $\sim$0.02 seconds satisfy the same condition.

There are a few things to mention about the method used. First, even though we corrected for difficulties in determining the best fit, we believe, partially due to the erratic behavior of the best fit paths, that the best fit may still not be estimated correctly. This is accounted for in the error bars. However, a better method of finding the best fit and more conservative error bars are worth considering. The location of the best fit may also not reflect the behavior of the entire modified gridsearch, which leads into a discussion on ongoing efforts and future plans.

We have developed an approach to assessing differences between modified and unmodified gridsearches that focuses on more averaged quantities. The method involves creating modified and unmodified likelihood gridsearches. We then integrate the unmodified likelihood gridsearch, and consider the area $A_{unmod}$ that makes up a percentage $P_{unmod}$ of it, say 90%. We then calculate the percentage $P_{mod}$ of the integrated modified gridsearch that falls within $A_{unmod}$ and plot $P_{mod}$ versus $P_{unmod}$. If the modified waveform were to be exactly the same as the unmodified one (i.e., we considered two unmodified waveforms), this "P-P" plot would be a diagonal line. We are currently working to produce these type of results for the same gridsearch parameters we have used so far. We expect to share all our results in some form, perhaps in a paper, within a year.

# Acknowledgements

I would like to thank Trevor Sidery, who daily provided the knowledge and patience to make this project possible. I would also like to thank Ilya Mandel, who propelled the project forward with his insight and guidance. Thanks go to Harald Pfeiffer and Jonathan Gair for their contributions to some very useful discussions. The helpfulness and kindness of the entire gravitational wave group

at the University of Birmingham made the IREU extremely enjoyable. Bernard Whiting, Guido Mueller, Kristin Nichola, Antonis Mytidis, and everyone else at the University of Florida were enormously helpful, and I am grateful to them for the creation and administration of the program. Matthew Semak and the rest of the physics program faculty at the University of Northern Colorado were instrumental in helping me prepare for the REU. I also appreciate the efforts of Tania Silver, who for two months waited while I worked on the other side of the world. Funding by the NSF made this IREU possible.

[1] P. Ajith, M. Hannam, S. Husa, Y. Chen, B. Bruegmann, N. Dorband, D. Mueller, F. Ohme, D. Pollney, C. Reisswig, L. Santamaria, and J. Seiler. Inspiral-merger-ringdown waveforms for black-hole binaries with non-precessing spins. *Phys. Rev. Lett.*, 106:241101, 2011.

[2] E. Baird, S. Fairhurst, M. Hannam, and P. Murphy. Degeneracy between mass and spin in black-hole-binary waveforms. *Phys. Rev. D*, 87:024035, 2012.

[3] C. Cutler and E. E. Flanagan. Gravitational waves from merging compact binaries: How accurately can one extract the binary's parameters from the inspiral waveform? *Phys. Rev. D*, 49:2658–2697, 1994.

[4] T. Damour and A. Nagar. Improved analytical description of inspiralling and coalescing black-hole binaries. *Phys. Rev. D*, 79:081503, 2009.

[5] M. Hannam, S. Husa, F. Ohme, and P. Ajith. Length requirements for numerical-relativity waveforms. *Phys. Rev. D*, 82:124052, 2010.

[6] I. MacDonald, A. H. Mroue, H. P. Pfeiffer, M. Boyle, L. E. Kidder, M. A. Scheel, B. Szilagyi, and N. W. Taylor. Suitability of hybrid gravitational waveforms for unequal-mass binaries. *Phys. Rev. D*, 87:024009, 2013.

[7] I. MacDonald, S. Nissanke, and H. P. Pfeiffer. Suitability of post-newtonian/numerical-relativity hybrid waveforms for gravitational wave detectors. *Class. Quantum Grav.*, 28:134002, 2011.

[8] Michele Maggiore. *Gravitational Waves: Volume 1: Theory and Experiments*. Oxford University Press, USA, 2007.

[9] F. Ohme. Analytical meets numerical relativity – status of complete gravitational waveform models for binary black holes. *Class. Quantum Grav.*, 29:124002, 2012.

[10] Y. Pan, A. Buonanno, M. Boyle, L. T. Buchman, L. E. Kidder, H. P. Pfeiffer, and M. A. Scheel. Inspiral-merger-ringdown multipolar waveforms of nonspinning black-hole binaries using the effective-one-body formalism. *Phys. Rev. D*, 84:124052, 2011.

[11] L. Santamaria, F. Ohme, P. Ajith, B. Bruegmann, N. Dorband, M. Hannam, S. Husa, P. Mosta, D. Pollney, C. Reisswig, E. L. Robinson, J. Seiler, and B. Krishnan. Matching post-newtonian and numerical relativity waveforms: Systematic errors and a new phenomenological model for nonprecessing black hole binaries. *Phys. Rev. D*, 82:064016, 2010.

[12] B. F. Schutz. Gravitational waves on the back of an envelope. *American Journal of Physics*, 52:412, 1984.

[13] D. Shoemaker. Advanced LIGO anticipated sensitivity curves, Jan 2010.

# Appendices

## A Best Fit Paths for Three-stage Modified IMRPhenomB Templates

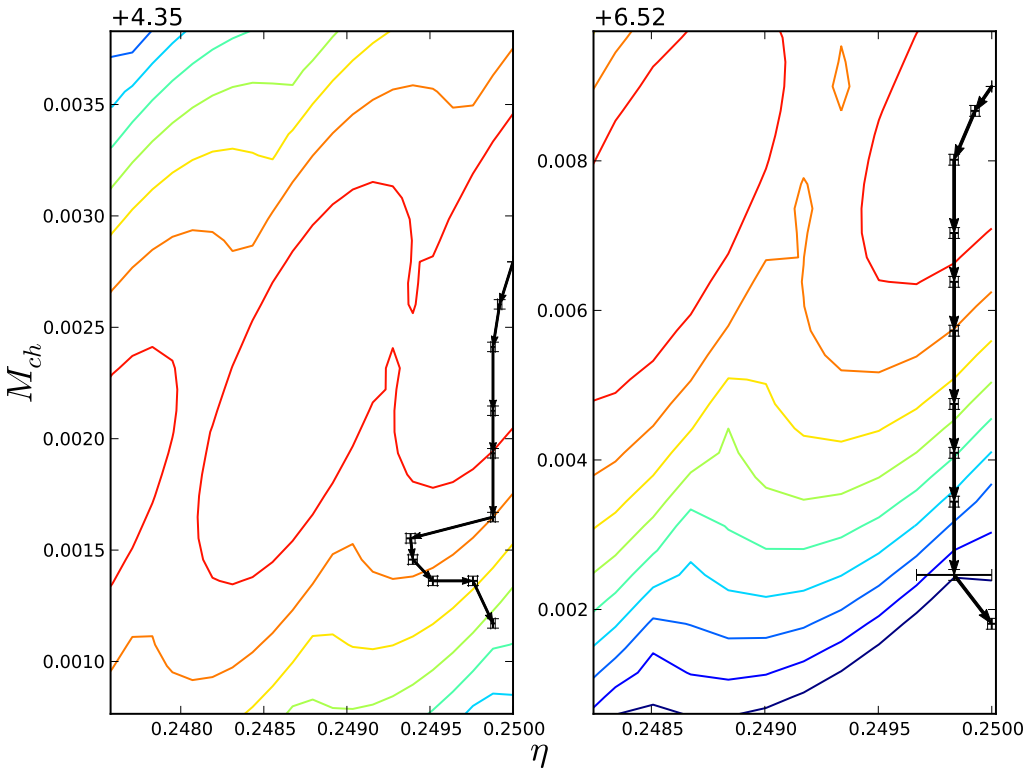


Figure 10: Best fit path plots for $M_{total}$ of 10 and 15 $M_{\odot}$ (left and right respectivly). We vary $\alpha$ from 0.0 to 1.0 rad in increments of 0.1 rad.

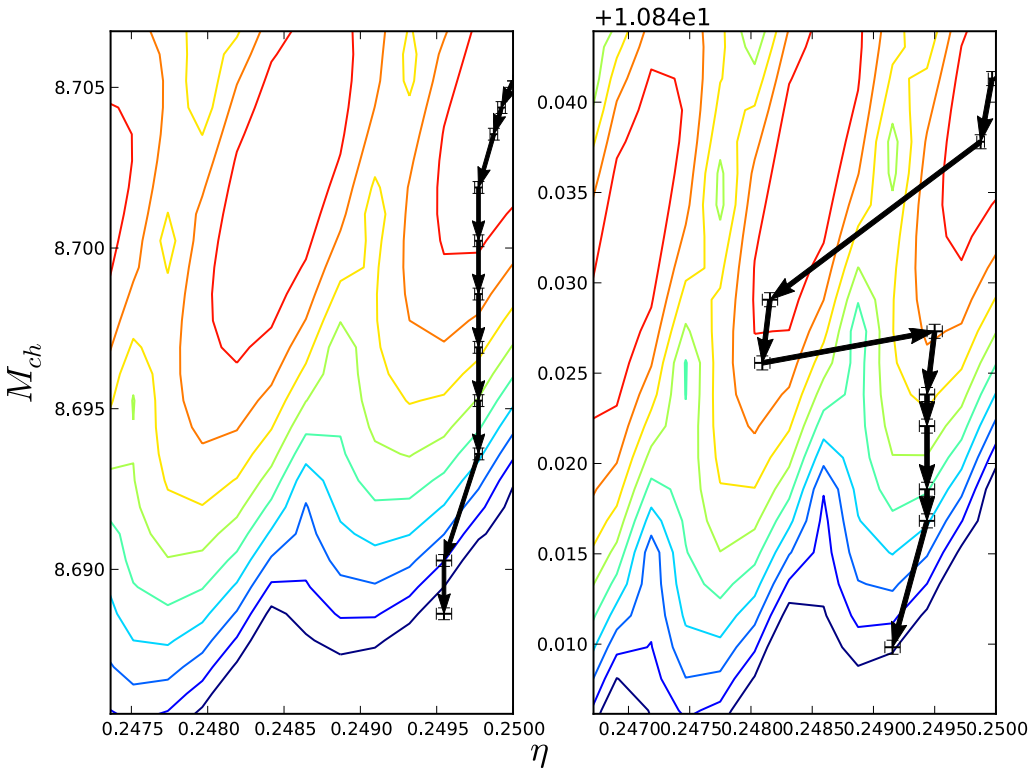


Figure 11: Best fit path plots for $M_{total}$ of 20 and 25 $M_{\odot}$ (left and right respectivly). We vary $\alpha$ from 0.0 to 1.0 rad in increments of 0.1 rad.

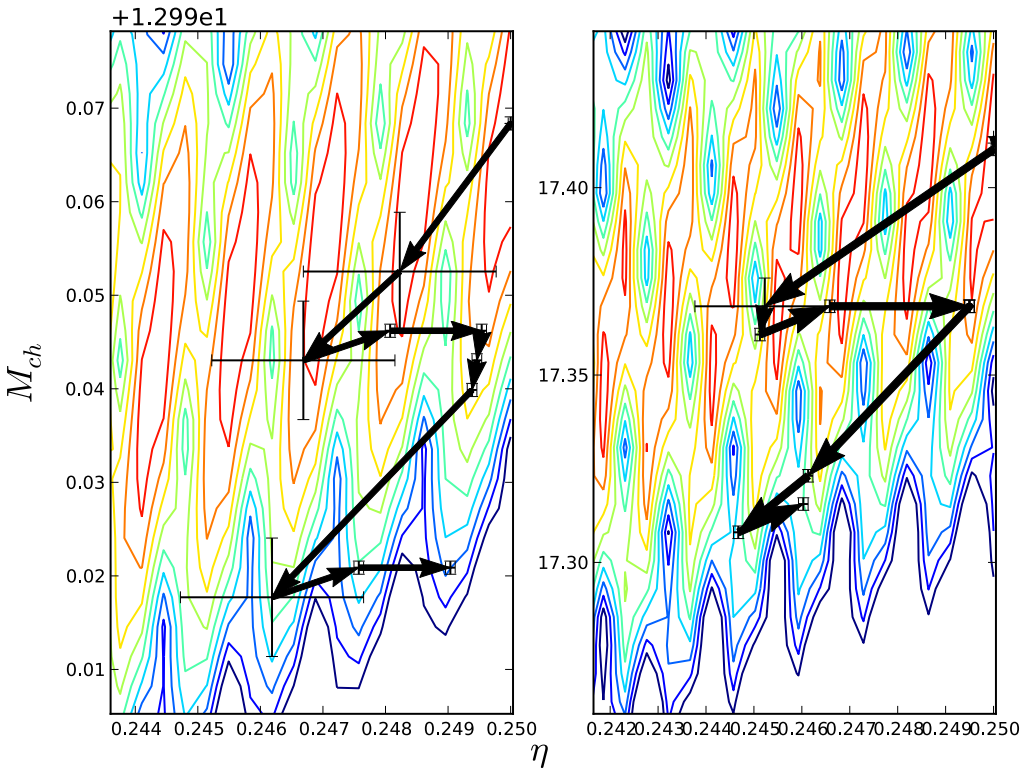


Figure 12: Best fit path plots for $M_{total}$ of 30 and 40 $M_{\odot}$ (left and right respectivly). We vary $\alpha$ from 0.0 to 1.0 rad in increments of 0.1 rad.

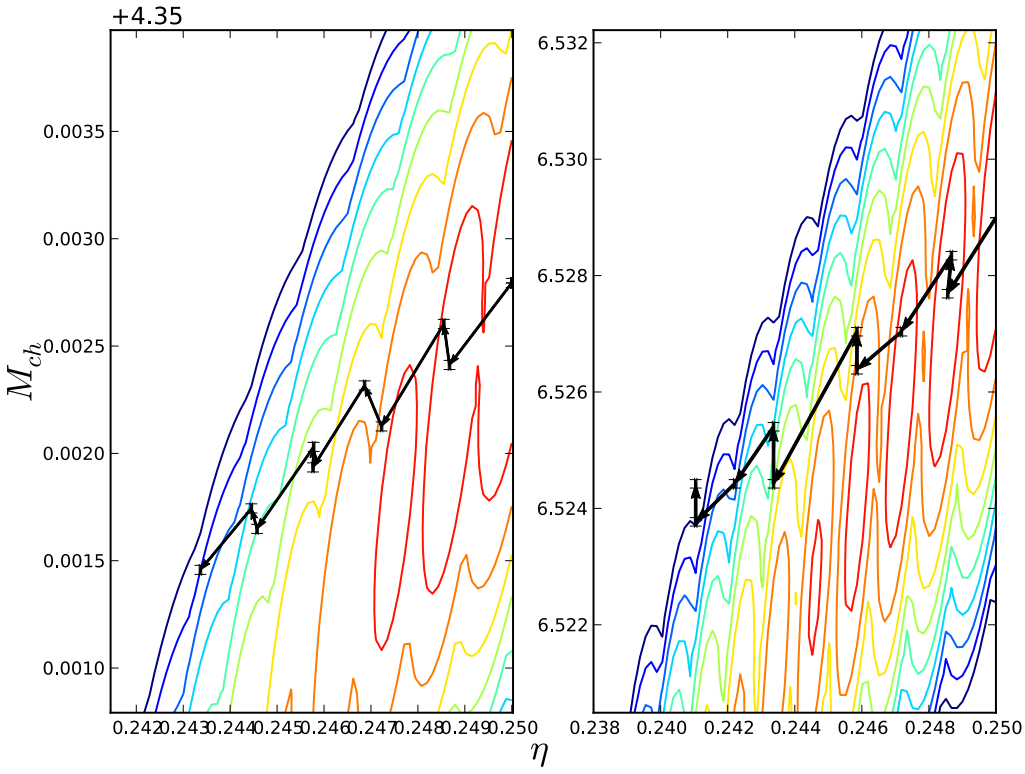


Figure 13: Best fit path plots for $M_{total}$ of 10 and 15 $M_{\odot}$ (left and right respectivly). We vary $\alpha$ from 0.0 to $-1.0$ rad in increments of 0.1 rad.

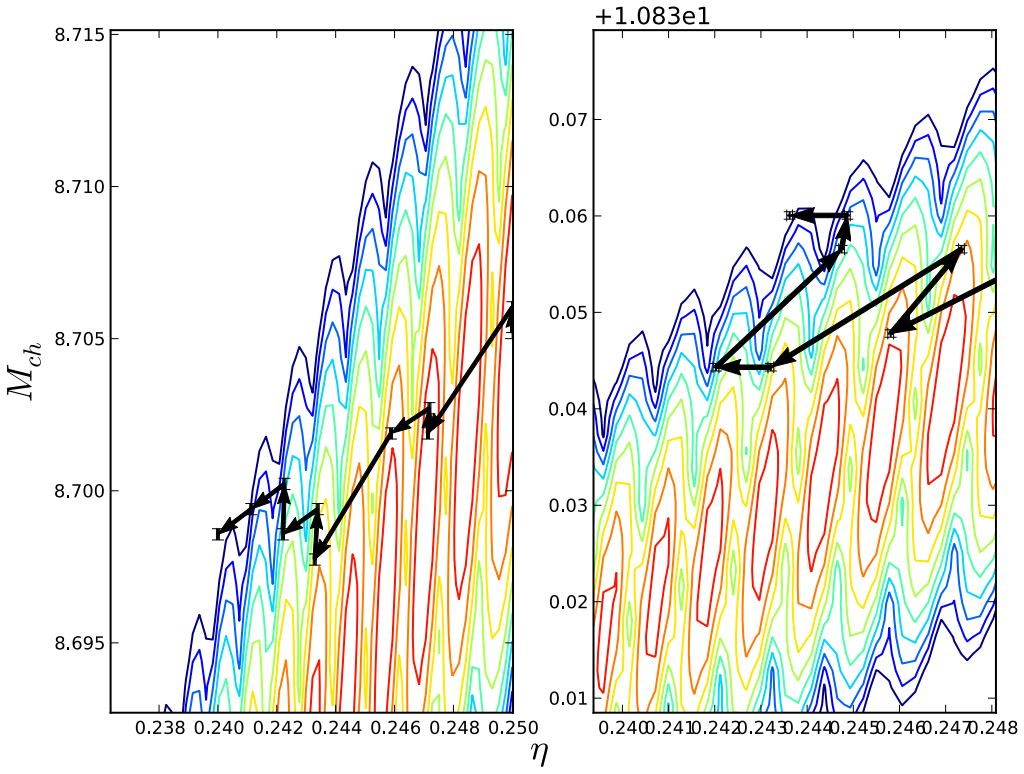


Figure 14: Best fit path plots for $M_{total}$ of 20 and 25 $M_{\odot}$ (left and right respectivly). We vary $\alpha$ from 0.0 to $-1.0$ rad in increments of 0.1 rad.

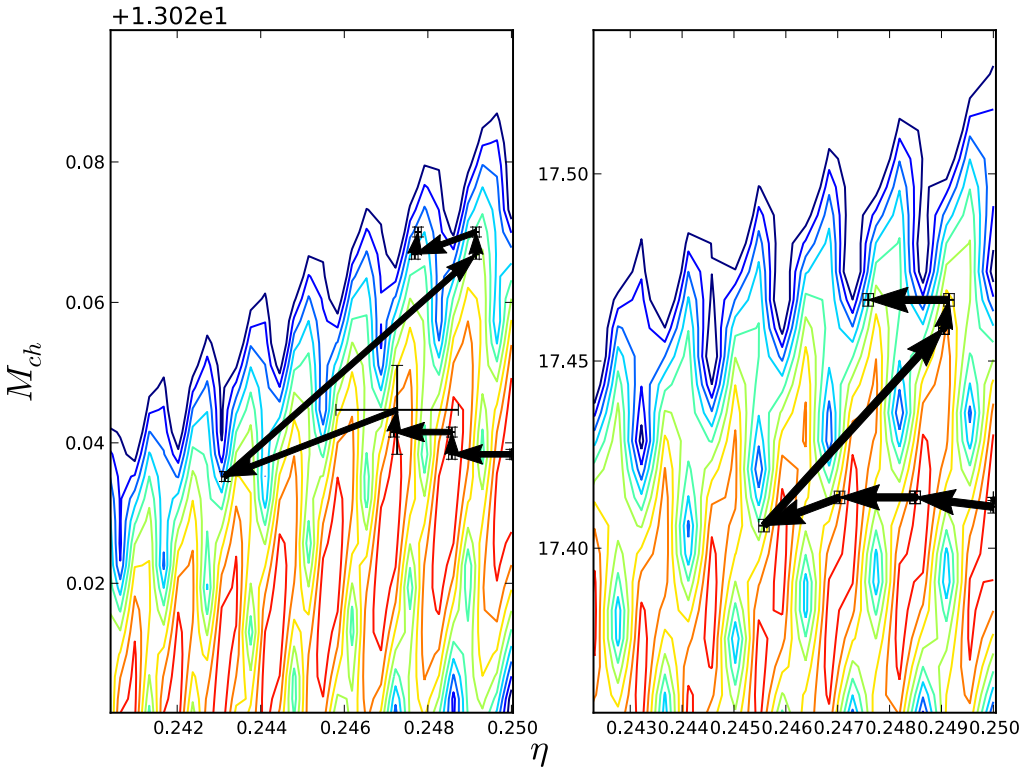


Figure 15: Best fit path plots for $M_{total}$ of 30 and 40 $M_{\odot}$ (left and right respectivly). We vary $\alpha$ from 0.0 to $-1.0$ rad in increments of 0.1 rad.

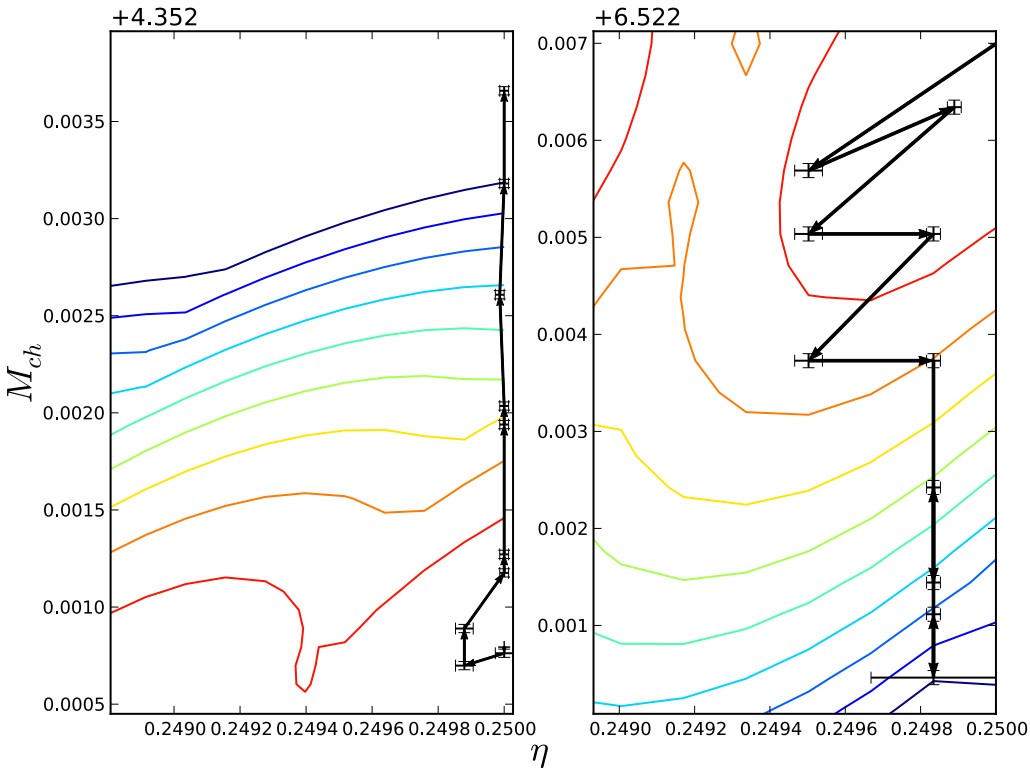


Figure 16: Best fit path plots for $M_{total}$ of 10 and 15 $M_{\odot}$ (left and right respectivly). We vary $\tau$ from 0.0 to 0.05 seconds in increments of 0.05 seconds.

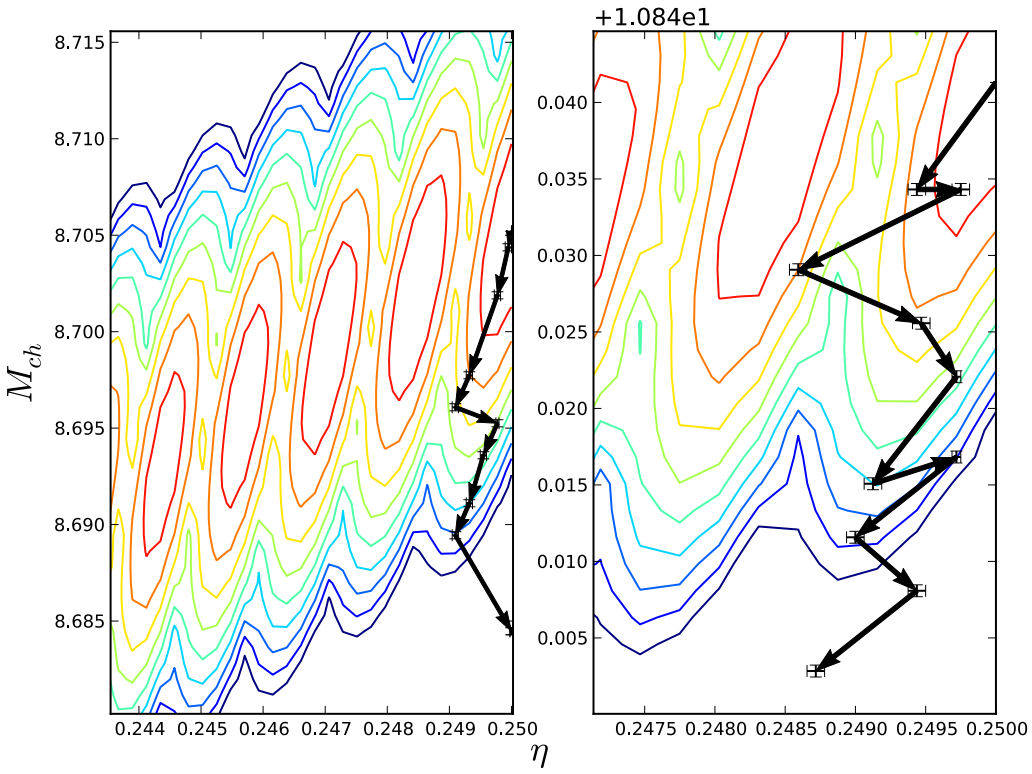


Figure 17: Best fit path plots for $M_{total}$ of 20 and 25 $M_{\odot}$ (left and right respectivly). We vary $\tau$ from 0.0 to 0.05 seconds in increments of 0.05 seconds.

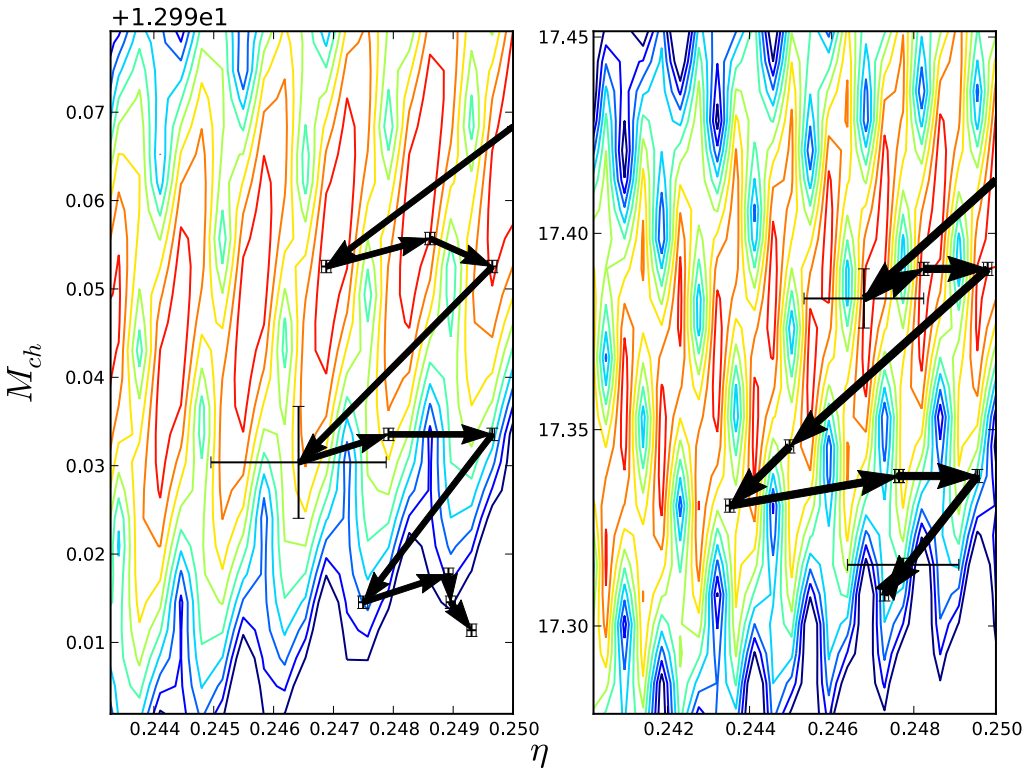


Figure 18: Best fit path plots for $M_{total}$ of 30 and 40 $M_{\odot}$ (left and right respectivly). We vary $\tau$ from 0.0 to 0.05 seconds in increments of 0.05 seconds.

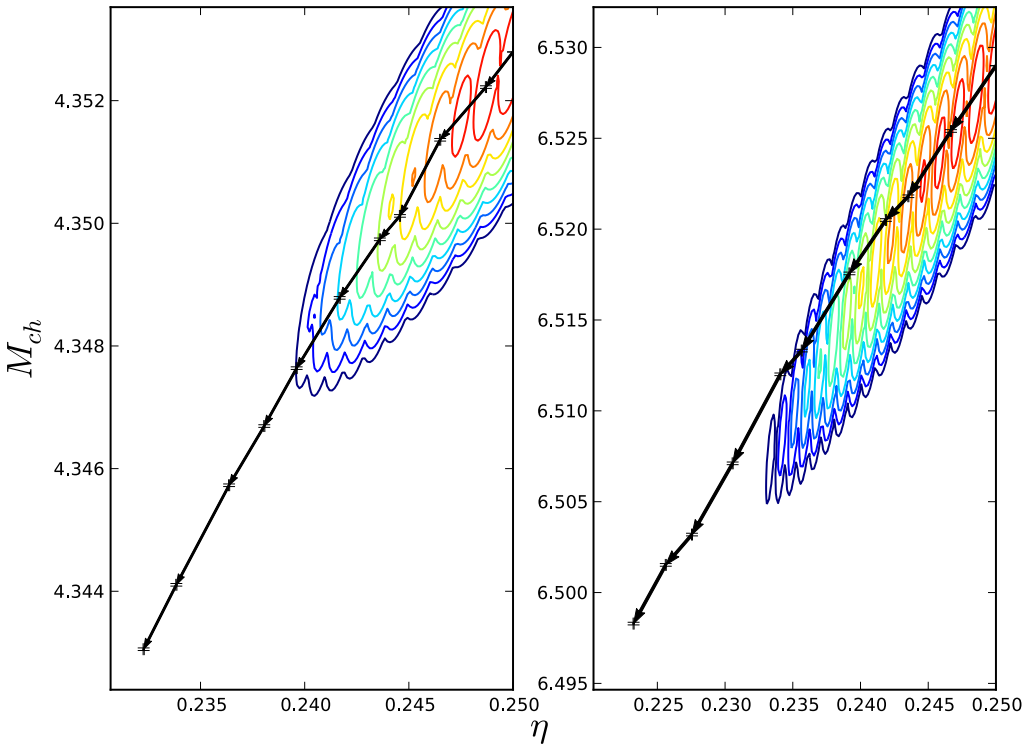


Figure 19: Best fit path plots for $M_{total}$ of 10 and 15 $M_{\odot}$ (left and right respectivly). We vary $\tau$ from 0.0 to $-0.05$ seconds in increments of 0.05 seconds.

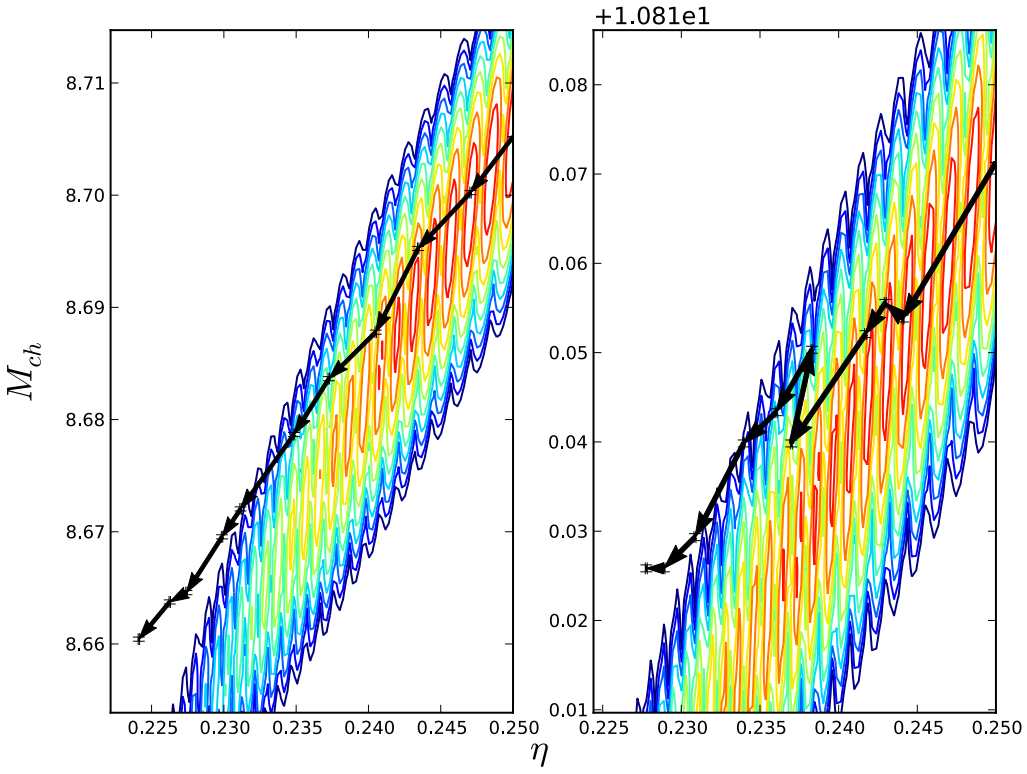


Figure 20: Best fit path plots for $M_{total}$ of 20 and 25 $M_{\odot}$ (left and right respectivly). We vary $\tau$ from 0.0 to $-0.05$ seconds in increments of 0.05 seconds.

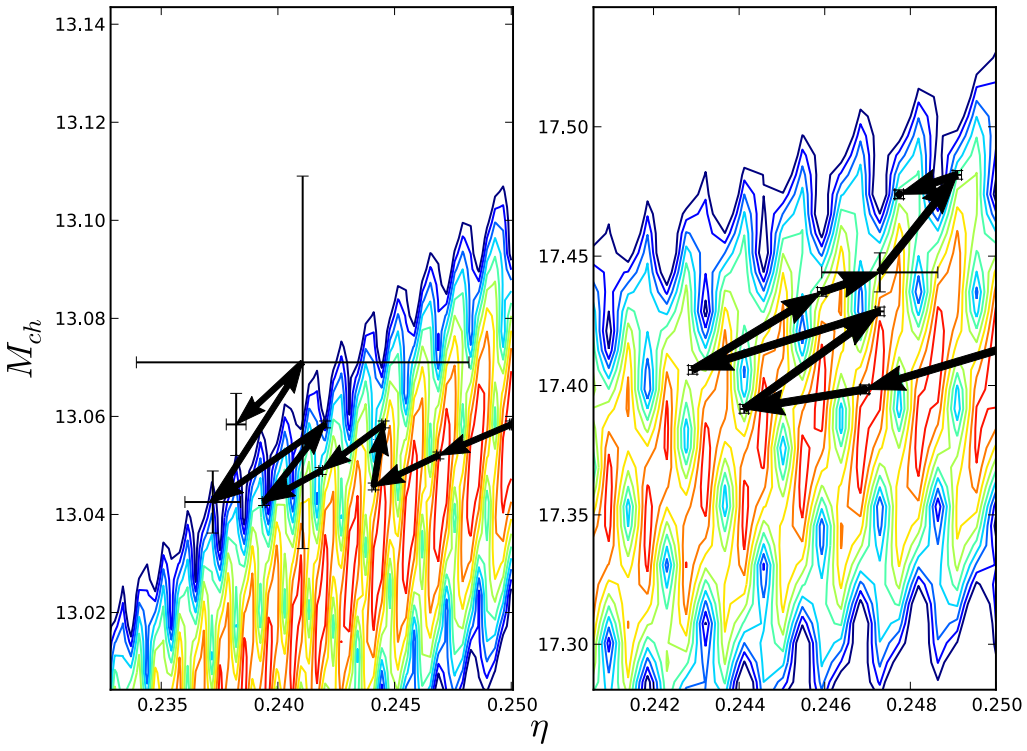


Figure 21: Best fit path plots for $M_{total}$ of 30 and 40 $M_{\odot}$ (left and right respectivly). We vary $\tau$ from 0.0 to $-0.05$ seconds in increments of 0.05 seconds.

# B Best Fit Paths for PN-term Modified IMRPhenomB Templates

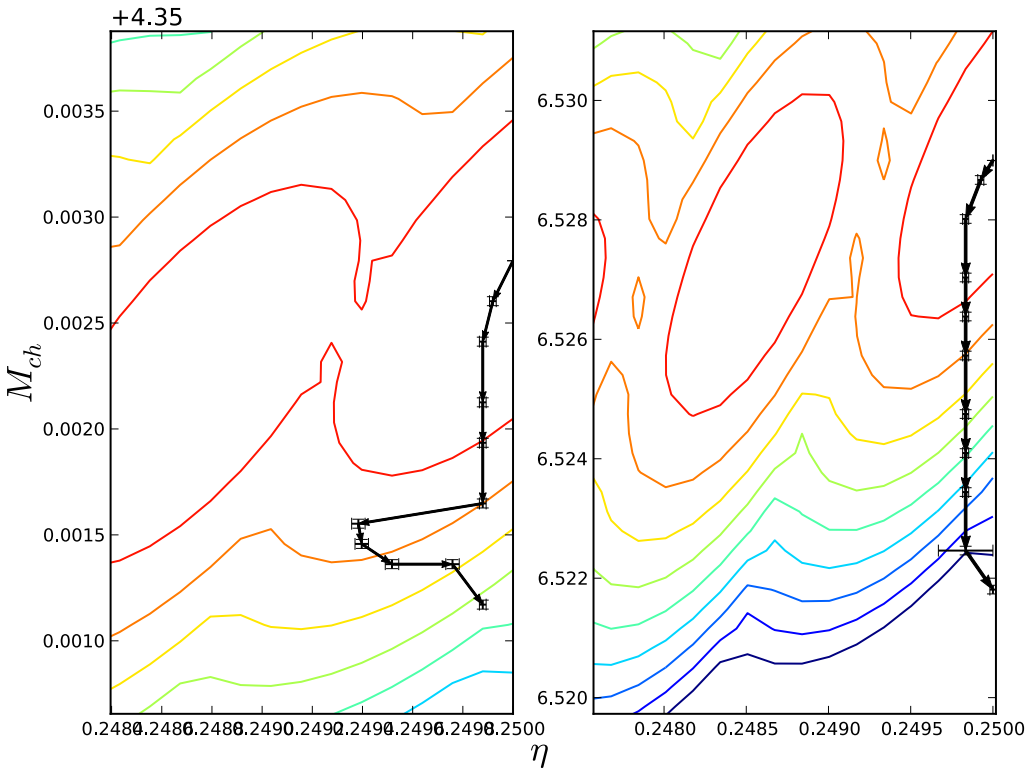


Figure 22: Best fit path plots for $M_{total}$ of 10 and 15 $M_{\odot}$ (left and right respectivly). We vary $\alpha_P$ from 0.0 to 1.0 rad in increments of 0.1 rad.

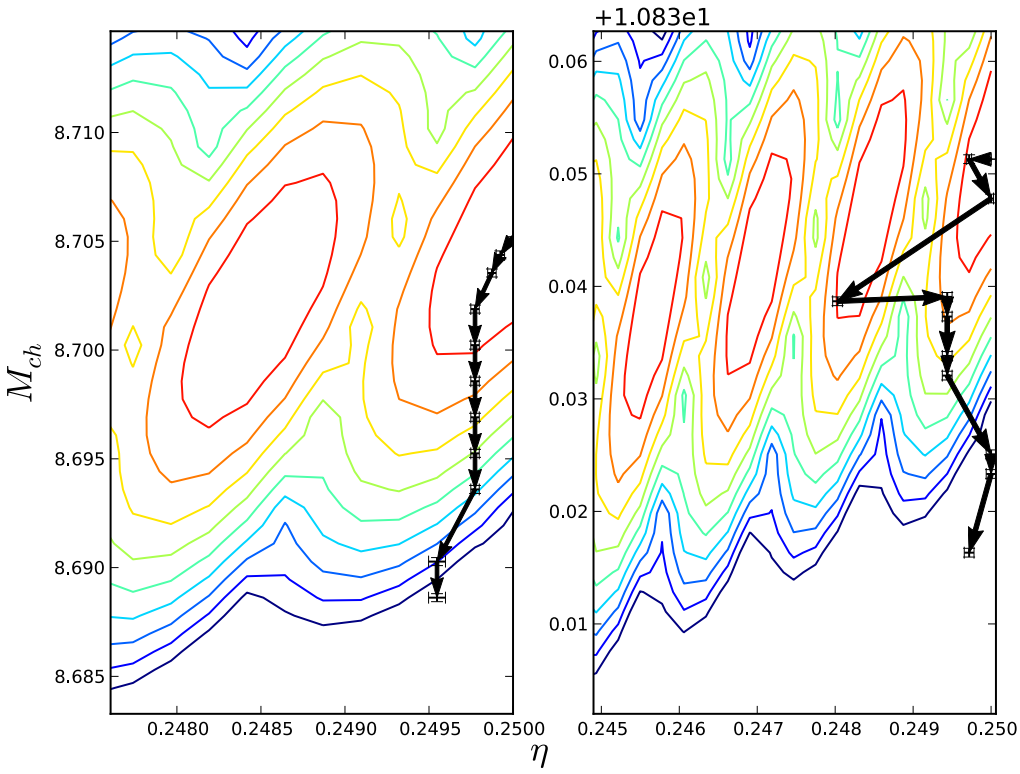


Figure 23: Best fit path plots for $M_{total}$ of 20 and 25 $M_{\odot}$ (left and right respectivly). We vary $\alpha_P$ from 0.0 to 1.0 rad in increments of 0.1 rad.

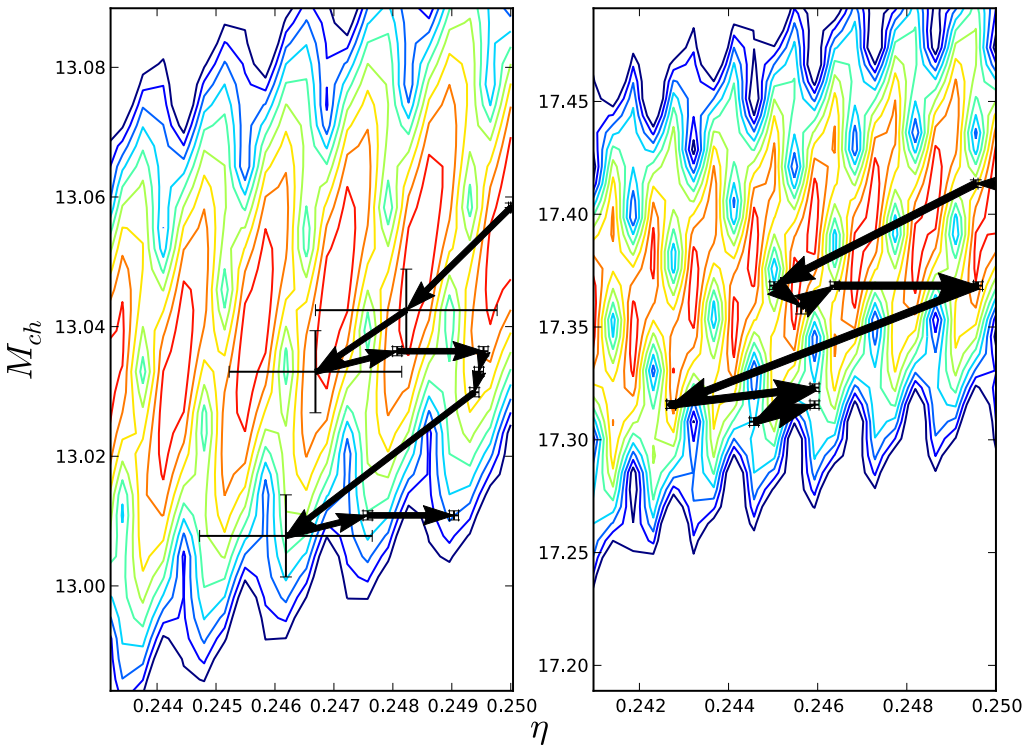


Figure 24: Best fit path plots for $M_{total}$ of 30 and 40 $M_{\odot}$ (left and right respectivly). We vary $\alpha_P$ from 0.0 to 1.0 rad in increments of 0.1 rad.

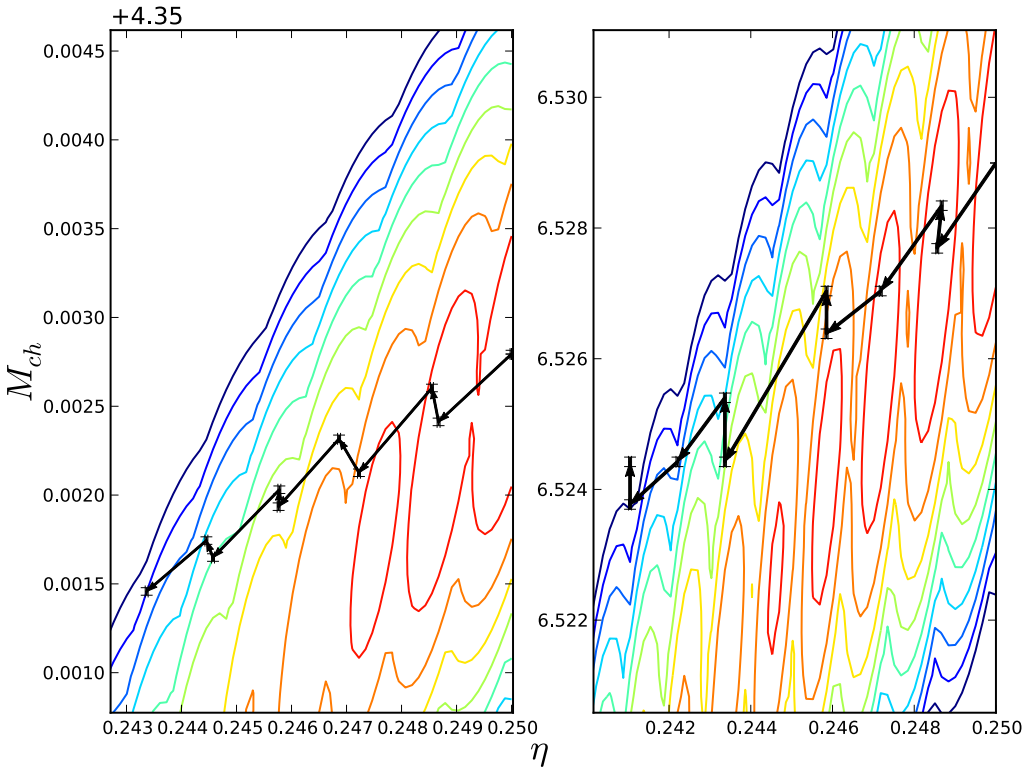


Figure 25: Best fit path plots for $M_{total}$ of 10 and 15 $M_{\odot}$ (left and right respectivly). We vary $\alpha_P$ from 0.0 to $-1.0$ rad in increments of 0.1 rad.

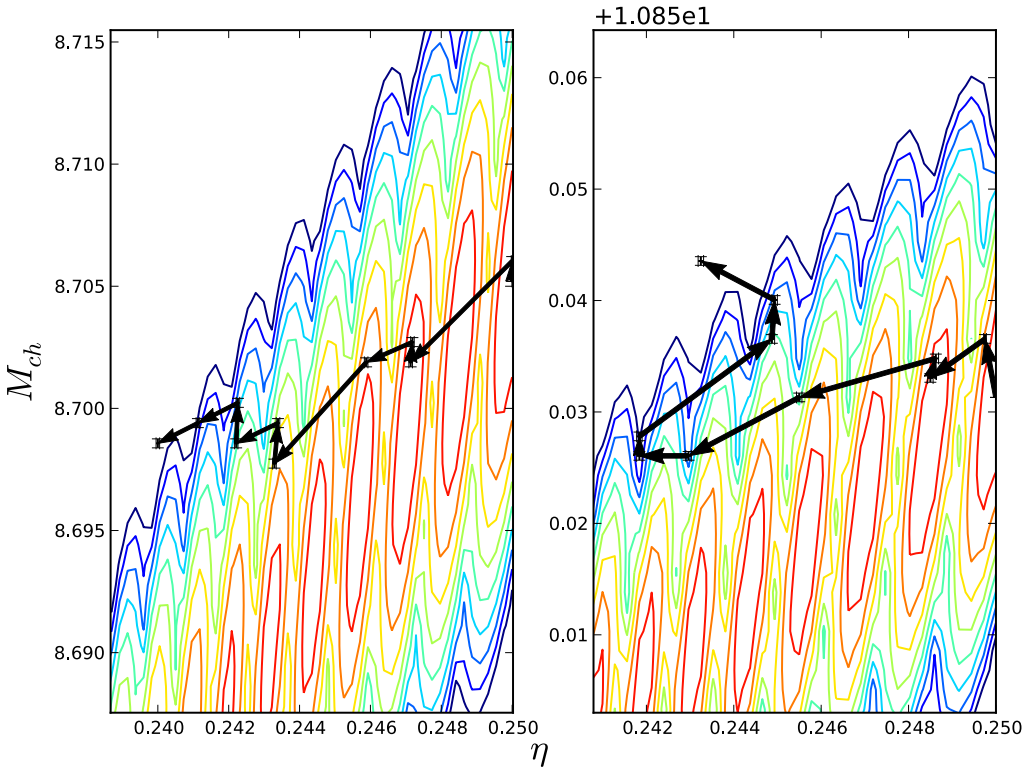


Figure 26: Best fit path plots for $M_{total}$ of 20 and 25 $M_{\odot}$ (left and right respectivly). We vary $\alpha_P$ from 0.0 to $-1.0$ rad in increments of 0.1 rad.

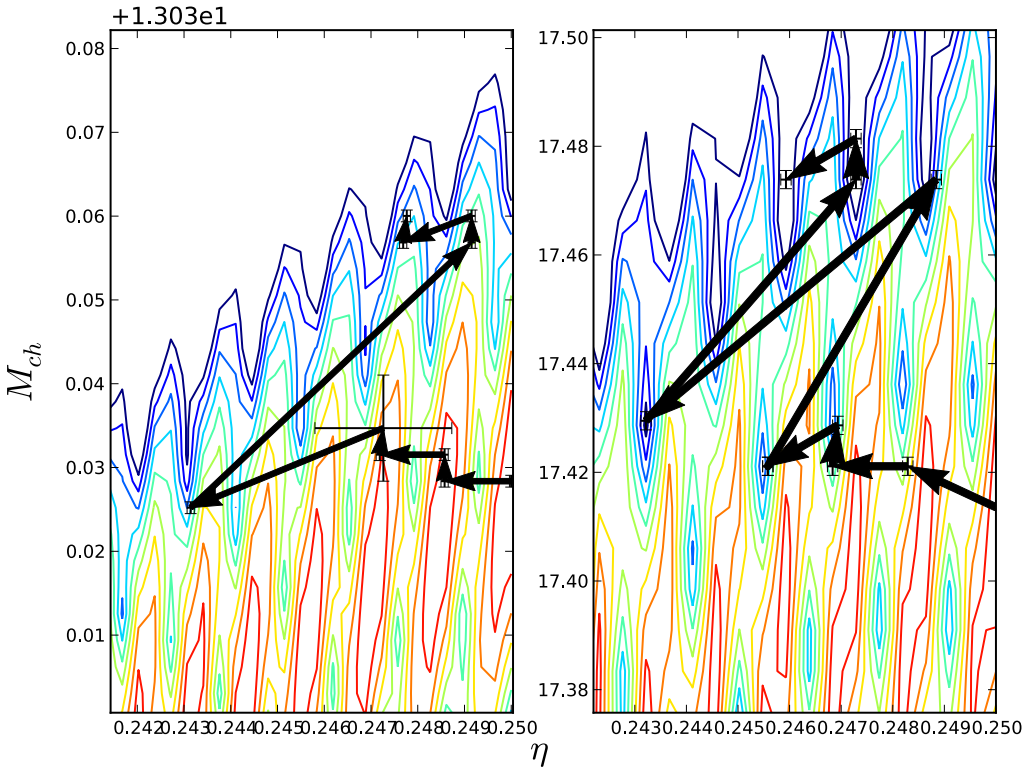


Figure 27: Best fit path plots for $M_{total}$ of 30 and 40 $M_{\odot}$ (left and right respectivly). We vary $\alpha_P$ from 0.0 to $-1.0$ rad in increments of 0.1 rad.